Am J Cancer Res 2023;13(10):4560-4578
www.ajcr.us /ISSN:2156-6976/ajcr0152613

Original Article

Single-cell analysis of castration-resistant prostate cancers to identify potential biomarkers for diagnosis and prognosis of neuroendocrine prostate cancer

Yung-Chih Hong[1*], Tze-Yun Hu[2*], Chih-Sin Hsu[3], Wayne W Yeh[2], Wei-Ze Wong[1], Tsai-Wen Shen[2], Ching-Hsin Chang[2,4], Kate Hua[3], Chien-Yi Tung[3], Yu-Ching Peng[5], William J Huang[1,6], Pei-Ching Chang[2,3], Tzu-Ping Lin[1,6]

[1]Faculty of Medicine, National Yang Ming Chiao Tung University, Hsinchu 30010, Taiwan; [2]Institute of Microbiology and Immunology, National Yang Ming Chiao Tung University, Hsinchu 30010, Taiwan; [3]Cancer Progression Research Center, National Yang Ming Chiao Tung University, Taipei 11221, Taiwan; [4]Department of Urology, Taipei Medical University Hospital, Taipei 11031, Taiwan; [5]Department of Pathology and Laboratory Medicine, Taipei Veterans General Hospital, Taipei 11217, Taiwan; [6]Department of Urology, Taipei Veterans General Hospital, Taipei 11217, Taiwan. [*]Equal contributors.

Received August 4, 2023; Accepted August 29, 2023; Epub October 15, 2023; Published October 30, 2023

Abstract: The high heterogeneity and low percentage of neuroendocrine cells in prostate cancer limit the utility of traditional bulk RNA sequencing and even single-cell RNA sequencing to find better biomarkers for early diagnosis and stratification. Re-clustering of specific cell-type holds great promise for identification of intra-cell-type heterogeneity. However, this has not yet been used in studying neuroendocrine prostate cancer heterogeneity. Neuroendocrine cluster(s) were individually identified in each castration-resistant prostate cancer specimen and combined for trajectory analysis. Three neuroendocrine states were identified. Neuroendocrine state 2 with the highest AR score was considered the initial starting state of neuroendocrine transdifferentiation. State 1 and state 3 with distinct high neuroendocrine scores and marker genes enriched in N-Myc and REST target genes, respectively, were considered as two different types of neuroendocrine differentiated cancer cells. These two states contained distinct groups of prostate cancer biomarkers and a strong distinguishing ability of normal versus cancerous prostate across different pathological grading was found in the N-Myc-associated state. Our data highlight the central role of N-Myc and REST in mediating lineage plasticity and classifying neuroendocrine phenotypes.

Keywords: Prostate cancer, castration-resistant, neuroendocrine, N-Myc, REST, single-cell RNA sequencing

Introduction

Prostate cancer (PCA) is the second most frequent malignancy diagnosed and the fifth leading cause of cancer death in men worldwide [1]. Although androgen deprivation therapy (ADT) remains the gold standard for treating patients with PCA [2], the disease often develops into castration-resistant prostate cancer (CRPC), associated with the restoration of androgen receptor (AR) signaling [3]. The prevalence of CRPC drove the development of second-generation AR pathway inhibitors, such as the androgen biosynthesis inhibitor abiraterone and the AR antagonist enzalutamide [4]. Unfortunately, the response to these new-generation therapies is only transient and patients eventually relapse with progression to a more aggressive form of PCA with neuroendocrine features, known as neuroendocrine prostate cancer (NEPC) [5, 6]. Thus, the incidence of NEPC has escalated after the wide use of second-generation AR-targeting therapy [7]. Given that treatment-induced NEPC no longer responds to AR-targeted therapy, as well as traditional chemotherapy [6], patients diagnosed with NEPC have a median overall survival of less than a year [7, 8]. Addressing the mechanisms of neuroendocrine differentiation (NED) will benefit the development of new diagnostic and thera-

peutic strategies to restore sensitivity to AR-targeted therapy.

Cellular plasticity has emerged as a fundamental developmental process that allows a single genotype to acquire polymorphisms in response to environmental stimuli [9] and has become an important mechanism facilitating treatment-induced drug resistance [10]. In line with this, accumulating evidence suggested that lineage plasticity may contribute to the acquisition of morphological characteristics and differentiation states of NEPC [11-13], a molecular feature characterized by reduced/no expression of AR signature markers and increased expression of neuroendocrine markers, such as chromogranin A (CgA), neuron-specific enolase (NSE), synaptophysin (SYP), and tubulin III (TUBIII) [8, 14]. Fortunately, the advent of next-generation sequencing (NGS) makes a comprehensive analysis of the molecular features of NEPC possible. Based on the bulk RNA-sequencing (RNA-seq) and DNA-sequencing (DNA-seq) data, neuroendocrine transdifferentiation in advanced CRPC is believed to be a consequence of epigenetic regulation of cellular plasticity rather than genomic alteration, as the fact that loss of RB1, TP53, and PTEN [8, 15, 16] and ERG translocation [17] were shared between CRPC adenocarcinoma (CRPC-adeno) and NEPC.

For epigenetic reprogramming in PCA, a pronounced example is that N-Myc drives a lineage switch in prostate adenocarcinoma toward a neural identity that favors the development of NEPC [12, 18]. In addition, we and others have previously identified REST (also known as neuron restrictive silencing factor; NRSF), a transcriptional repressor of neuronal genes in neural precursor cells and non-neuronal cells, as another epigenetic driver for NEPC progression. Since NEPC is characterized by the expression of genes associated with the neural lineage [8], the amplification/overexpression of N-Myc [18-20] and the loss of REST [21-23] have been considered as crucial routes for the acquisition of neuroendocrine phenotype in PCA. However, whether N-Myc and REST may, alone or cooperatively, initiate the epigenetic reprogramming of NEPC is largely unknown. Demonstrating the unique and critical contribution of N-Myc and REST in the progression of NEPC will benefit the development of therapeutic strategies to restore sensitivity to AR-targeted therapy. Moreover, NEPC is an end-stage lethal subtype of CRPC with fundamental problems in early and accurate diagnosis [24, 25]. Early detection of NEPC or detection of CRPC-adeno cells undergoing NED offers the prospect of a better prognosis. Identification of marker genes in N-Myc and REST-associated NEPC states may also help develop new diagnostic biomarkers for NEPC.

Single-cell RNA-seq (scRNA-seq) has created an unprecedented opportunity to simultaneously assess the transcriptional profiles of thousands of individual cells in a sample, enabling an unbiased display of heterogeneity among tumor cells [26, 27]. Several recent studies have successfully used scRNA-seq to demonstrate the heterogeneity of human PCA tissues [28-32]. Ma and Song *et al.* revealed the heterogeneity of primary PCA and discovered novel biomarkers for the diagnosis of early-stage PCA [28] and cell states associated with carcinogenesis [29], respectively. Chen *et al.* detected the heterogeneity of tumor microenvironment in 12 primary and 1 metastatic PCA tissues [32]. He *et al.* showed the expression of AR isoforms in mediating resistance to AR-targeting therapy in metastatic CRPC [33]. Taking advantage of scRNA-seq in providing unique opportunities to detect rare subpopulations, Dong and Wang *et al.* detected neuroendocrine tumor cells in CRPC specimens and try to identify their origin [30, 31]. Since a detailed analysis of neuroendocrine cells in metastatic CRPC at single-cell resolution is still lacking, we used scRNA-seq to profile the transcriptomes of 6,512 single cells of lymph node metastatic CRPC (mCRPC) tissue and found that it consisted of four major AR-positive luminal groups and a minor group comprising ~1% of neuroendocrine positive luminal cells. In line with previous reports showing REST as a NED repressor [21-23], we found that REST-targeted genes increased significantly in the neuroendocrine-positive group when compared to AR-positive adenocarcinoma cells. To in-depth investigate the heterogeneity of NEPC, we combined public datasets and identified 2,903 luminal cells positive for neuroendocrine markers from CRPC samples from five patients. Using trajectory analysis, we found that NEPC cells consisted of three distinct states. The AR and neuroendocrine scoring suggested that state 2 re-

presents the initial starting state within the 3 states of NEPC cells. Combining GSEA and biomarker genes, we found N-Myc and REST as key epigenetic regulators of state 1 and state 3, respectively. Notably, we found that N-Myc-driven NEPC exhibited high specificity and sensitivity in distinguishing high-grade PCA from normal prostate, showed significant abilities to predict disease-free survival, and may relate to drug resistance of CRPC, while REST-driven NEPC seems relatively benign. In summary, our findings revealed the heterogeneity of NEPC at the single-cell level and uncovered a state of N-Myc-regulated cells that could be critical for the diagnosis and stratification of PCA.

Materials and methods

Human subject

The patient was first diagnosed with metastatic prostate adenocarcinoma at 56-year-old with a clinical stage of TNM of cT4N1M1b and a prostate-specific antigen (PSA) level of 1,302 ng/ml. Computed tomography (CT) scan and bone scan showed lymph node and bone metastases. The patient was treated with first-line ADT (leuprolide and bicalutamide) for 14 months and then diagnosed with CRPC as his PSA levels increased. After being diagnosed with CRPC, the patient was treated with chemotherapy for 4 months. The lymph node mCRPC tissue used in this study was collected from the same patient at the age of 60-year-old. The stage of cTNM was cT4N1M1b with a PSA level of 745 ng/ml. The lymph node specimen displayed a cellular morphology resembling NEPC and positive for the neuroendocrine markers SYP and CD56/NCAM1. Informed consents were obtained from the patient and experiments with human subjects were approved by the Institutional Review Board (IRB) of Taipei Veterans General Hospital (TVGH).

Single-cell suspension preparation

A surgically removed lymph node from a PCA patient was immersed in MACS Tissue Storage Solution (Miltenyi Biotec, cat. no. 130-100-008) and immediately transported to the laboratory on ice. The tissue block was placed in a sterile Petri dish containing 5 ml of EpiGRO™ Human Prostate Epithelia Basal Medium (Millipore, cat No. SCMP-BM) and minced into small cubes (~1 mm). The pieces were transferred to a gentleMACS C tube (Miltenyi Biotec, cat. no. 130-093-237) containing 5 ml of digestive enzymes from Human Tumor Dissociation Kit (Miltenyi Biotec, cat. no. 130-095-929) diluted in EpiGRO™ Human Prostate Basal Medium. Then, a single-cell suspension was made with a gentleMACS Octo Dissociator (Miltenyi Biotec, cat. no. 130-096-427) using the h_TDK_2 program. The sample was incubated at 37°C under continuous gentle shaking. After completion of the run, 5 ml of EpiGRO Human Prostate Basal Medium was added to the gentleMACS C tube and then the single cell suspension was filtered through a 70-μm cell strainer (FALCON, cat. no. 352350). Viable cells were isolated by Ficoll density gradient centrifugation (1000×g at room temperature for 15 min). Cell number and cell viability were determined with a Countess II FL Automated Cell Counter (Invitrogen, cat No. AMQAF1000). Finally, the single-cell suspension was centrifuged at 300×g at 4°C for 7 min and resuspended at a density of 1000 cells/μl in EpiGRO™ Human Prostate Basal Medium prior to immediate scRNA analysis.

Single-cell library preparation and sequencing

The single-cell suspension, which has viability greater than 90%, was loaded onto the 10× Genomics Single-Cell-A Chip for target capture of ~10,000 cells/chip. The cDNA library was prepared using Chromium Next GEM Single Cell 3' Reagent Kits v3.1 (10× Genomics, cat. no. PN-1000121), according to the manufacturer's protocol. The library was sequenced on a NovaSeq 6000 (Illumina, cat. no. 20012850) at a depth of ~150 M reads.

Single-cell data processing and cell-type annotation

Raw sequencing data was processed by the Cell Ranger (10× Genomics, version 3.1.0) analysis pipeline, followed by alignment to the human reference genome (GRCh38). Cells with low-quality cell barcodes or with high percentage of reads that mapped to the mitochondrial genome were excluded. The DoubletFinder was used to detect and remove potential doublets. The 6,512 high-quality cells were included for further analysis using Partek Flow (Partek, cat. no. 4485102). Gene counts were normalized by $\log_2$(CPM+1) and genes that are not expressed in more than 99.9% of cells were

excluded. Seurat3 integrated method was applied to remove the batch effect across the samples.

The cells that passed the quality control were clustered by Graph-based clustering and visualized by t-distributed stochastic neighbor embedding (t-SNE). Cell-type annotation for each cluster is based on the expression of marker genes for different cell-type: epithelial cell (EPCAM, KRT8, KRT5, and CDH1), endothelial cell (ENG, VWF, and CDH5), myeloid cell (CD14, CD68, and AIF1). Epithelial cells are divided into two types: luminal cell (KRT8 and KRT18) and basal cell (KRT5 and KRT14).

Biomarker genes identification and gene ontology (GO) enrichment analysis

Biomarker genes were identified using the compute biomarkers function in Partek Flow and selected a fold change ≥ 2 and a *p*-value < 0.05. Biomarker genes were subjected to GO analysis using ingenuity pathway analysis (IPA) software (QIAGEN).

Trajectory analysis

The 2,903 neuroendocrine cells identified in five CRPC specimens were used to construct the trajectory analysis with Monocle2 using default parameter in Partek Flow. The biomarker genes of States 1, 2, and 3 were used to perform the GO enrichment analysis.

Clinical relevance

To determine the correlation of the top 10 biomarker genes in States 1 and 3 with the disease-free survival rates of PCA patients from TCGA, Kaplan-Meier curves were plotted for patients sorted according to the expression profiles (high versus low expression) of biomarker genes in top and bottom 20%. Gene Expression Profiling Interactive Analysis (GEPIA) (http://gepia.cancer-pku.cn/index.html) was used for data processing. The Mantel-Cox test was used to calculate the logarithmic rank *p*-value.

Gene set enrichment analysis (GSEA)

GSEA (version 4.0.3) was used to analyze pathway enrichment. First, to evaluate the characteristic of biomarker genes, biomarkers were subjected to enrichment analysis using GSE5641 and GSE8702 from the Gene Expression Omnibus (GEO) database. Second, to evaluate the association of REST, N-Myc, and NKX2-1 with different states, the NRSF_01, MYCN_01, and TTF1_Q6 gene sets from GSEA MSigDB were subjected to enrichment analysis using the dataset from our scRNA-seq.

Results

Single-cell RNA sequencing (scRNA-seq) profiling and cell typing of a metastatic CRPC (mCRPC)

Given that focal NED has never been in-depth studied in advanced mCRPC at the single-cell level, we aimed to perform an scRNA-seq on this difficult-to-acquire high-quality specimen. In this study, we isolated a high percentage of viable cells (> 90%) from surgically removed inguinal lymph node tissue of a recurrent PCA patient who had received ADT treatment with combined leuprolide and bicalutamide. Using pathological immunohistochemistry (IHC) staining, the inguinal lymph node specimen was diagnosed as PCA by positive for prostate specific antigen (PSA), prostate specific membrane antigen (PSMA) and NKX3.1. The single cell suspension from this mCRPC tissue was then subjected to 10X Genomics Chromium based scRNA sequence (**Figure 1A**). After exclusion of dead cells as well as cells not passing quality control, we obtained a total of 6,512 high-quality cells with an average of ~3,900 gene features detected per cell. The cellular composition was explored with unsupervised graph-based clustering and visualized by t-SNE (**Figure 1B**). Using canonical marker genes curated from the literature [30, 34, 35], we manually classified seven cell clusters into three major cell types, including epithelial cells, endothelial cells, and myeloid cells (**Figure 1C**). Given that PCA is usually characterized by luminal cell expansion, we next evaluated the identities of the five epithelial clusters with luminal markers keratin 8 (KRT8) and keratin 18 (KRT18) and basal markers keratin 5 (KRT5) and keratin 14 (KRT14). The high expression of luminal markers (**Figure 1D**), but low to no expression of basal markers (data not shown), clearly indicated that all prostate epithelial clusters identified in our mCRPC specimen are luminal cells.

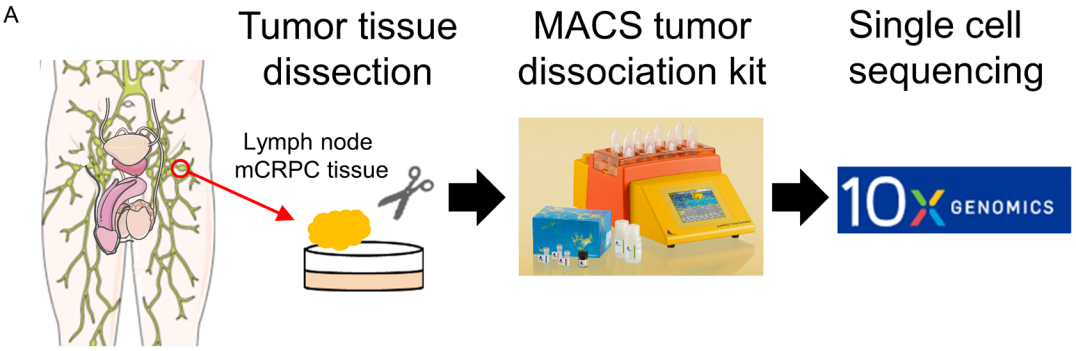

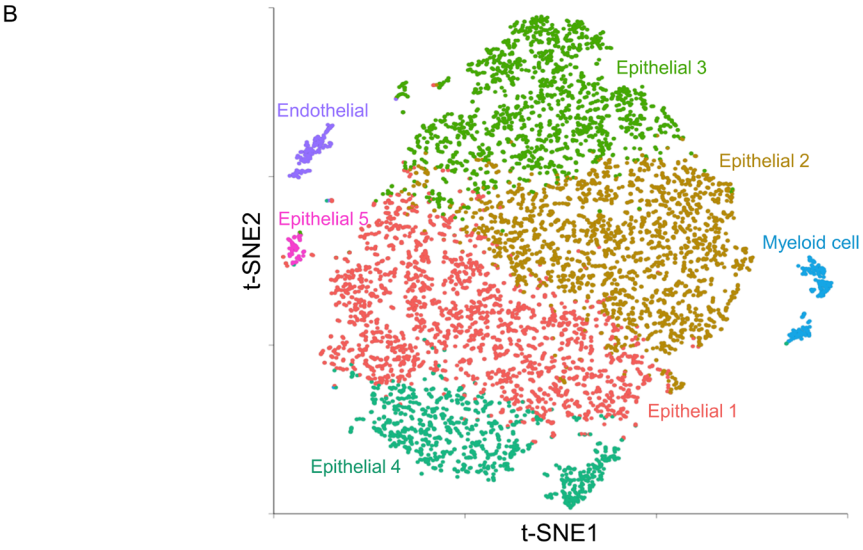

C

Cluster	Cell Number	Percentage
Epithelial 1	1985	30.48%
Epithelial 2	1886	28.96%
Epithelial 3	1453	22.31%
Epithelial 4	846	12.99%
Myeloid cell	163	2.50%
Endothelial cell	129	1.98%
Epithelial 5	50	0.77%

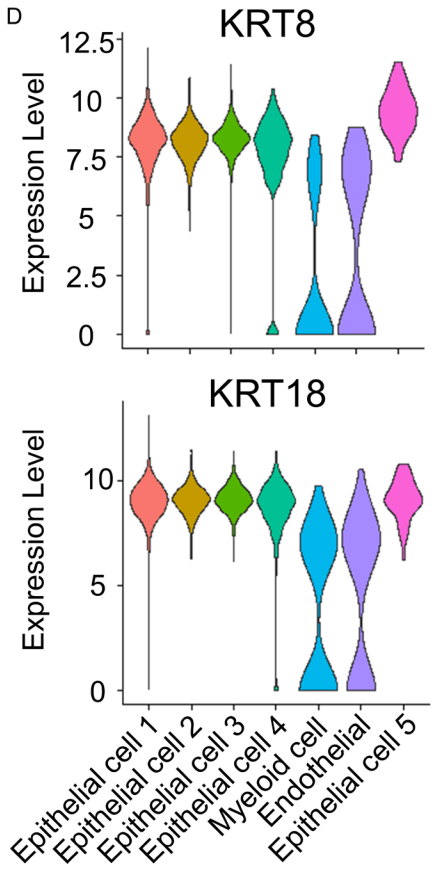

Figure 1. Dissection of cell types in lymph node metastatic CRPC (mCRPC) with single-cell RNA sequencing (scRNA-seq) analysis. A. Workflow of metastatic lymph node collection, tumor dissection, sequencing, and data analysis. B. T-distributed stochastic neighbor embedding (t-SNE) plot of 6,512 single cells, colored by assigned cell type. C. The cell numbers and percentages of each cluster. D. The violin plots display the expression of luminal marker genes KRT8 and KRT18 in each cluster.

Identification and characterization of neuroendocrine cells in mCRPC

Having characterized the luminal phenotype in all epithelial clusters, we next focused on studying the luminal compartment by computationally combining all luminal cells and then performed unsupervised graph-based clustering and visualized by t-SNE. The 6,220 luminal cells were divided into 5 clusters with 2 minor populations (**Figure 2A** and **2B**). Given that CRPC-adeno and NEPC can be broadly identified by prostate luminal (AR, KLK3) and neuroendocrine (CHGA, SYP) lineage markers, respectively, the expression levels of marker genes in each cluster were visualized by violin plot (generated with the VlnPlot package). The results showed that most luminal cells (luminal clusters 1 to 4) are CRPC-adeno, with a minor population (luminal cluster 5) representing an obvious neuroendocrine phenotype (**Figure 2C**), illustrating an intra-tumoral focal NED in mCRPC.

Using bulk RNA-seq data from 98 treatment-refractory mCRPC, Labrecque *et al.* have previously divided neuroendocrine-associated genes into REST-repressed genes (NEURO I) and transcription factors (NEURO II) [23]. The expression levels of REST in each cluster were visualized by violin plot (**Figure 2D**). Using the transcriptomic signature developed by Labrecque *et al.* in 2019, we showed that luminal 5 was NEPC cells without AR activity and expresses all REST-repressed neuroendocrine-associated genes (NEURO I) and part of the NEURO II transcription factors (**Figure 2E**). To further confirm the association of REST with NEPC cells, we performed GSEA using the NRSF_01 gene set. The result showed that the REST-targeted genes increased significantly in NEPC cells (luminal 5) when compared to CRPC-adeno cells (luminal 1-4) (**Figure 2F**), suggesting that luminal 5 neuroendocrine characteristics came from loss of REST activity. Since NEPC is AR-independent, we further performed GSEA using microarray datasets from LNCaP cells before versus after androgen deprivation (GSE8702). Consistently, the result showed that NEPC population (luminal 5) had an androgen-independent characteristic (**Figure 2G**).

To elucidate the functional properties of NEPC population, we performed a GO functional enrichment analysis of 2,916 biomarker genes ($P < 0.05$, ≥ 2-fold change) in luminal 5 using ingenuity pathway analysis (IPA). Consistent with the neuronal nature of NEPC, biomarkers in luminal 5 were enriched for development of neuron, organization of cytoskeleton and cellular protrusions (**Figure 2H**). Furthermore, biomarkers in luminal 5 were also positively enriched for cell transformation, movement, migration, and invasion (**Figure 2H**), supporting the high malignant and metastatic propensity of NEPC [36]. Having characterization of the metastatic phenotype of NEPC population, we further performed GSEA using microarray dataset that compares the expression profiles of cells undergone transendothelial migration *in vitro* or metastasis *in vivo* (GSE56410). Consistently, NEPC population (luminal 5) showed the metastatic characteristic (**Figure 2I**).

Elucidate the heterogeneity of NEPC population in CRPC

NEPC is a minor population even in CRPC. This is supported by our scRNA-seq data showing that NEPC (luminal 5) possess only 1.05% (65 cells) of luminal cells (**Figure 2B**). In keeping with our aim of characterizing the features of NEPC, we next downloaded GEO scRNA sequencing data from four CRPC samples with NED phenotype (GSE137829) [30]. We first performed unsupervised graph-based clustering and assigned luminal cells using its lineage markers (KRT8, KRT18). Clusters with > 60% of KRT8-positive and KRT18-positive cells were selected and combined for further analysis (Figure S1).

To collect NEPC cells in an unbiased manner, we first conducted an unsupervised graph-based clustering of luminal cells in the five CRPC. Secondly, we sought to identify neuroendocrine clusters using the expression levels of NEURO I and NEURO II markers [23]. Using Seurat scoring strategy, neuroendocrine cell populations were detected in our mCRPC (Pt1 CRPC) and the other four CRPC samples. In line with the result observed by Dong *et al.*, most clusters in Pt2 CRPC (GSE137829 patient #2) and Pt4 CRPC (GSE137829 patient #5) are neuroendocrine cells and a few clusters in Pt3 CRPC (GSE137829 patient #4) and Pt5 CRPC (GSE137829 patient #6) are neuroendocrine-

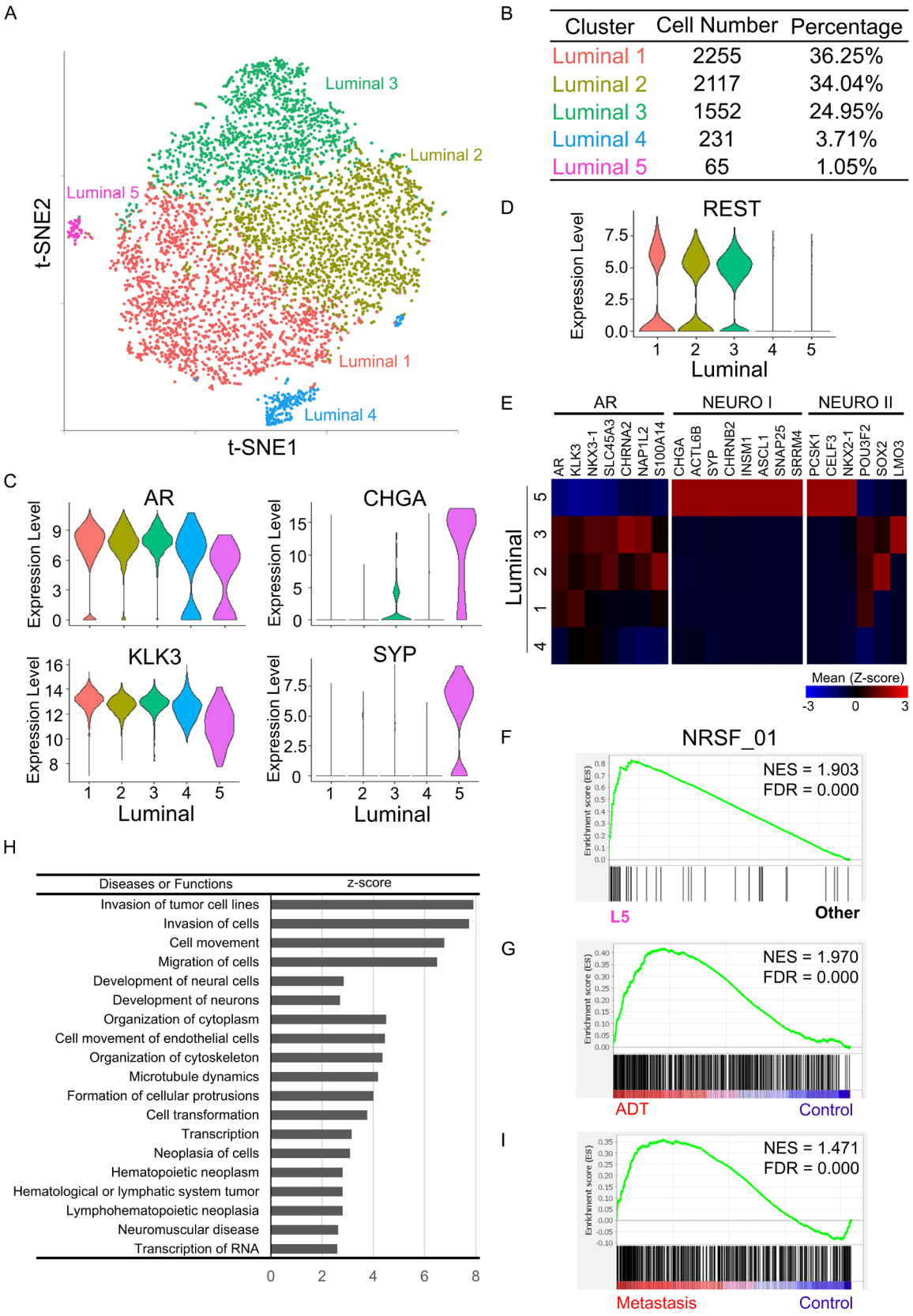

Figure 2. The luminal cells were grouped into five clusters. A. Luminal cells were combined and grouped into five clusters by graph-based clustering and demonstrated using a t-SNE plot. B. The number of cells and percentages of

five luminal clusters. C. The violin plots display the expression of androgen receptor (AR) signaling markers AR and PSA/KLK3 and neuroendocrine markers CHGA and SYP in each cluster. D. The violin plots display the expression of REST in each cluster. E. Heatmap generated based on the expression levels of the AR panels (AR-associated genes), NEURO I panels (neuroendocrine genes repressed by REST), and NEURO II panels (neuroendocrine transcription factors) in each luminal cluster. F. NRSF_01 gene set was subjected to GSEA enrichment analysis using scRNA-seq data of luminal cluster 5 in compared to all other groups. G. The luminal 5 biomarker genes were subjected to GSEA enrichment analysis using GSE56410 dataset. H. Ingenuity pathway analysis (IPA) was used to reveal functional categories significantly enriched in luminal 5 biomarker genes. I. Biomarker genes of luminal 5 were subjected to a GSEA enrichment analysis using GSE8702 dataset.

positive (**Figure 3**). Notably, we found that although most luminal cells from Pt2 CRPC and Pt4 CRPC represent an obvious NED phenotype, NEPC populations (cluster 1-4) in Pt2 CRPC contain both NEURO I and NEURO II markers, while NEPC populations (cluster 1, 2, 4, 5) in Pt4 CRPC contain mainly NEURO II markers (**Figure 3**, lower two rows). Pt3 CRPC, the PCA representing the early state of NED of adenocarcinomas toward neuroendocrine fate [30], has a NEURO I-positive cluster (cluster 6) and a NEURO II-positive cluster (cluster 5) (**Figure 3**, lower two rows of the middle column). Similar to our sample, Pt5 CRPC contains only one NEURO I-positive cluster (cluster 5), which has a relatively higher NEURO I score (> 2) (**Figure 3**, lower two rows of the right column). These results illustrate clear inter- and intratumoral heterogeneity regarding NED.

The trajectory analysis revealed distinct NEPC states

Given the relatively small population of NEPCs, the heterogeneity of NEPC has never been studied at the single-cell level. More importantly, NED may be governed by multiple epigenetic regulation mechanisms. To elucidate the heterogeneity of NEPC and its corresponding epigenetic regulation at the single-cell level, we first need to distinguish the different transcriptional states of NEPC cells. To this end, we combined the neuroendocrine clusters identified in each of the five CRPC samples (**Figure 3**) and then performed a monocle trajectory analysis. The trajectory analysis revealed three distinct cell states (**Figure 4A**), which highlighted the heterogeneous subpopulations of NEPC in CRPC. Given that neuroendocrine transdifferentiation is characterized by the loss of AR signaling and gain of neuroendocrine features, we next calculated AR, NEURO I and NEURO II scores for individual cells in each state. The non-neuroendocrine luminal clusters identified in the five CRPC samples were combined and used as luminal control. Consistent with neuroendocrine features with lower AR signaling, violin plot showed that all three states of NEPC populations have lower AR scores when compared to luminal cells (**Figure 4B**).

Interestingly, we noted that state 2 was mainly composed of neuroendocrine cells from Pt3 CRPC (**Figure 4A**). In line with the result observed by Dong *et al.* showing that Pt3 CRPC represents the early state of NED [30], NEPC state 2 showed a higher AR score when compared with states 1 and 3, while state 1 and state 3 have higher NEURO II and NEURO I scores when compared with state 2, respectively (**Figure 4B**). The data here indicate that state 2 may represent the initial starting state of NEPC. More importantly, NEPC cells split into two states at the end of state 2. State 3 comprises neuroendocrine cells from all CRPC samples, while state 1 contains neuroendocrine cells mainly from Pt2 CRPC and Pt4 CRPC, the two CRPC samples possess an obvious NED phenotype in most luminal cells (**Figure 4A**).

Identifying distinct NED-associated epigenetic regulatory mechanisms

Given that Labrecque *et al.* highlight the central role of REST in NEURO I and transcription factors, including CELF3, PCSK1, SOX2, POU3F2, LMO3, and NKX2-1, in NEURO II, we compared the expression levels of these epigenetic regulators in different states of NEPC from the scRNA-seq data. The most dramatic findings were the reduced expression of REST in state 3 (**Figure 5A**) and the increased expression of NKX2-1/TTF1, but not the other NEURO II transcription factors, in state 1 (**Figure 5B**). To further characterize the association of REST with state 3 and NKX2-1 with state 1, we performed GSEA using the NRSF_01 (REST) and TTF1_Q6 (NKX2-1) gene set, respectively. GSEA confirmed a highly significant enrichment of REST-targeted genes in state 3 versus state 2 (**Figure**

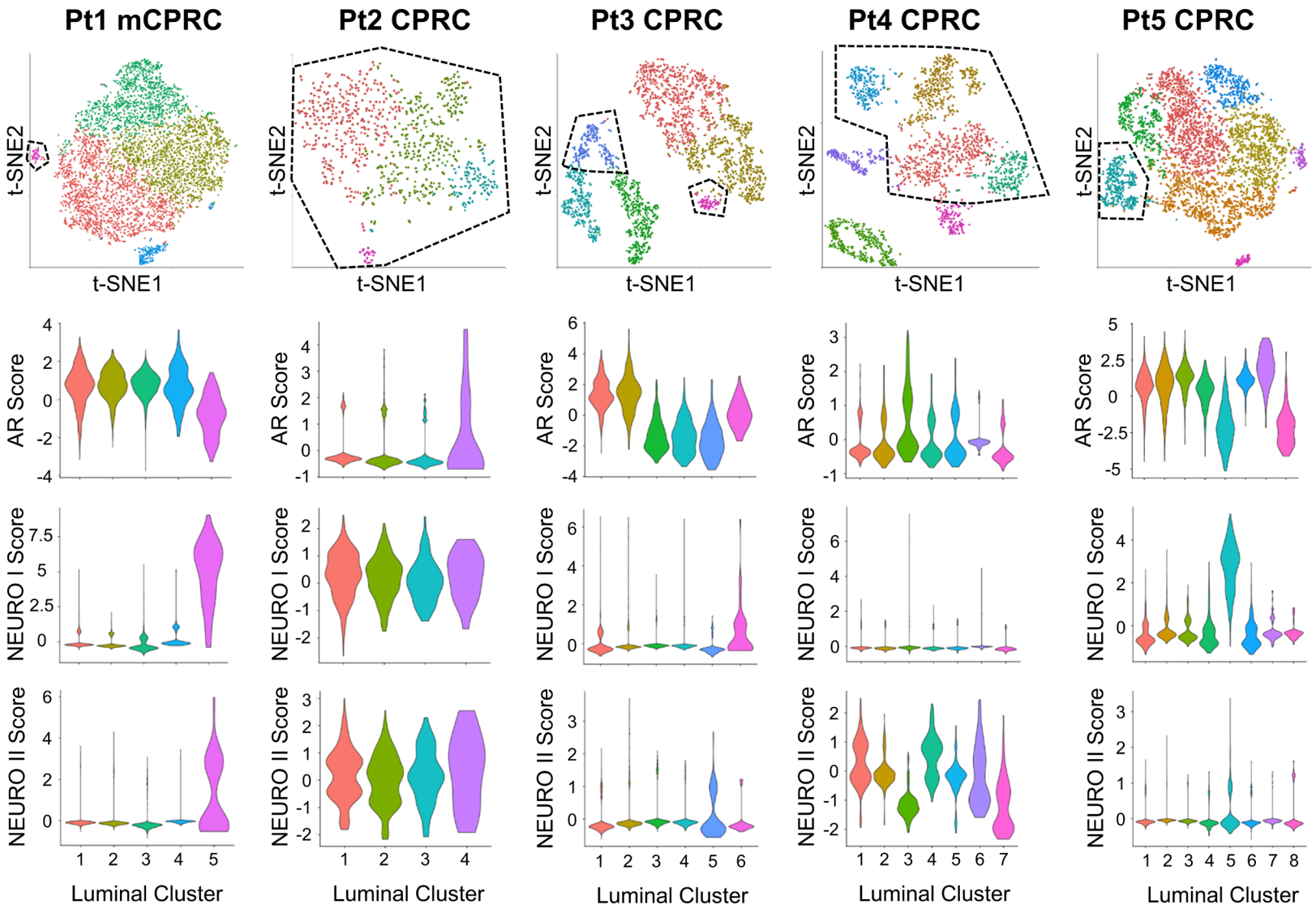

Figure 3. Identification of neuroendocrine cells from six human CRPC. A t-SNE plot of luminal cells from five patients (upper row) and violin plots showing AR, NEURO I and NEURO II scores using the well-established AR and neuroendocrine marker genes (lower rows). The violin plots display the score of AR panels (AR-associated genes), NEURO I panels (neuroendocrine genes repressed by REST), and NEURO II panels (neuroendocrine transcription factors) in luminal clusters of each sample. The areas marked with dotted lines are high-neuroendocrine-score cell populations (upper row).

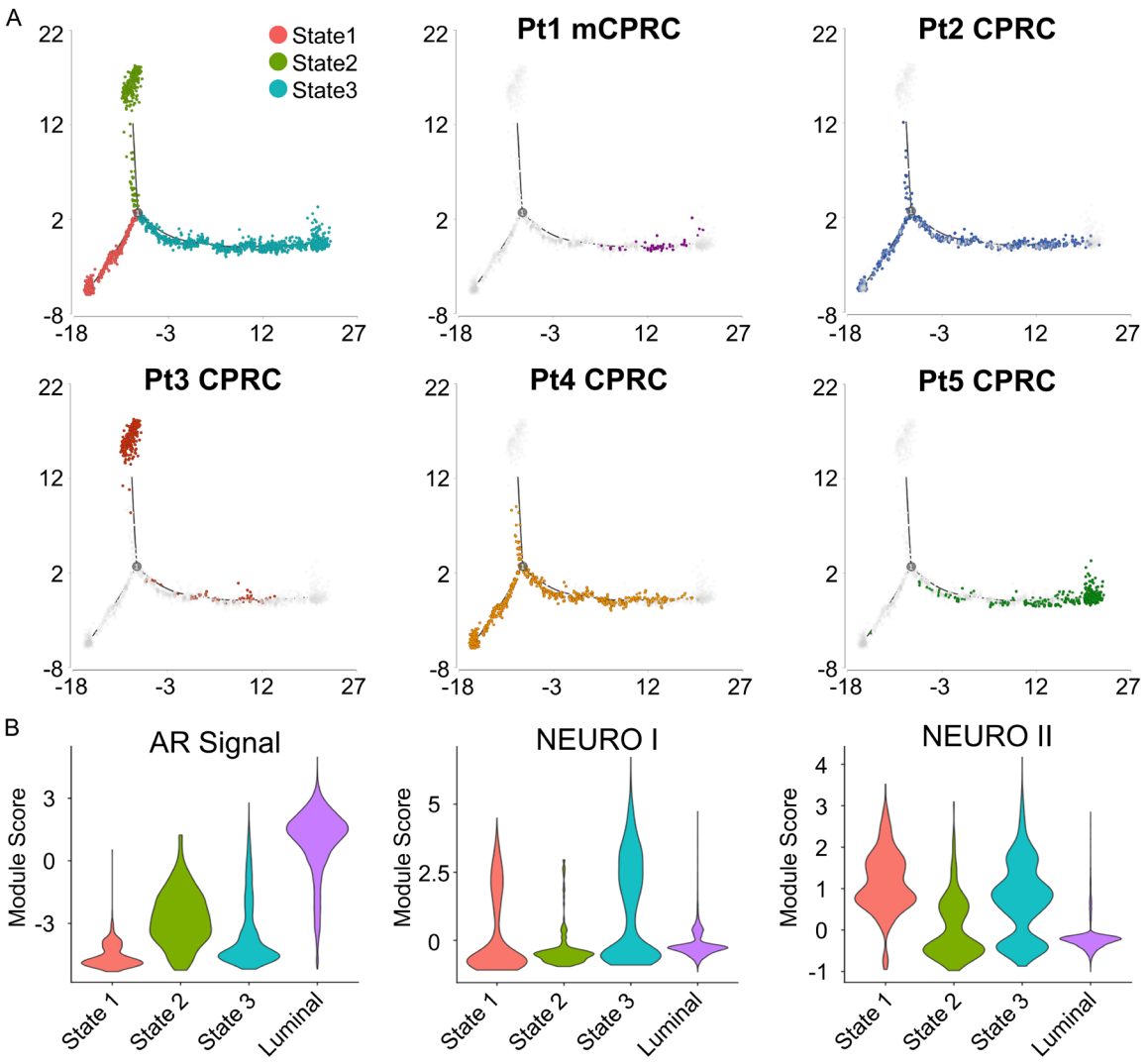

Figure 4. The trajectory analysis of neuroendocrine cells. A. Trajectory plot of neuroendocrine cells with color code indicates different states and specimens. B. The violin plots display the score of AR panels (AR-associated genes), NEURO I panels (REST-repressed neuroendocrine genes), and NEURO II panels (neuroendocrine transcription factors) in states 1, 2, 3 and the luminal group.

5C) and a slight but significant enrichment of genes associated with NKX2-1- in state 1 versus state 2 (**Figure 5D**). This suggests that the NEURO I feature of state 3 may mainly come from the loss of REST activity, while the NEURO II feature of state 1 may only partially result from the induction of NKX2-1.

Considering that N-Myc is one of the most well-known neuroendocrine-associated transcription factors in PCA [12, 18-20, 37] and NKX2-1 is its downstream target [12], we next detected its expression in different states of NEPC. However, it may be that due to the low expression level of master transcription activators, we were unable to detect N-Myc in the scRNA-seq data (**Figure 5E**). Therefore, we next use GSEA to study the enrichment of N-Myc target genes (NMYC_01) in state 1 or state 3 versus state 2. Consistent with our hypothesis, a significant enrichment of N-Myc target genes was found in state 1, but not in state 3 (**Figure 5F**). To further validate the association of N-Myc with state 1, we scored the correlation of N-Myc and transcription factors in NEURO II, including NKX2-1, with biomarkers enriched in state 1 and state 3 using the TCGA dataset. Among the 401 biomarkers in state 1 (Table S1), 392 genes were

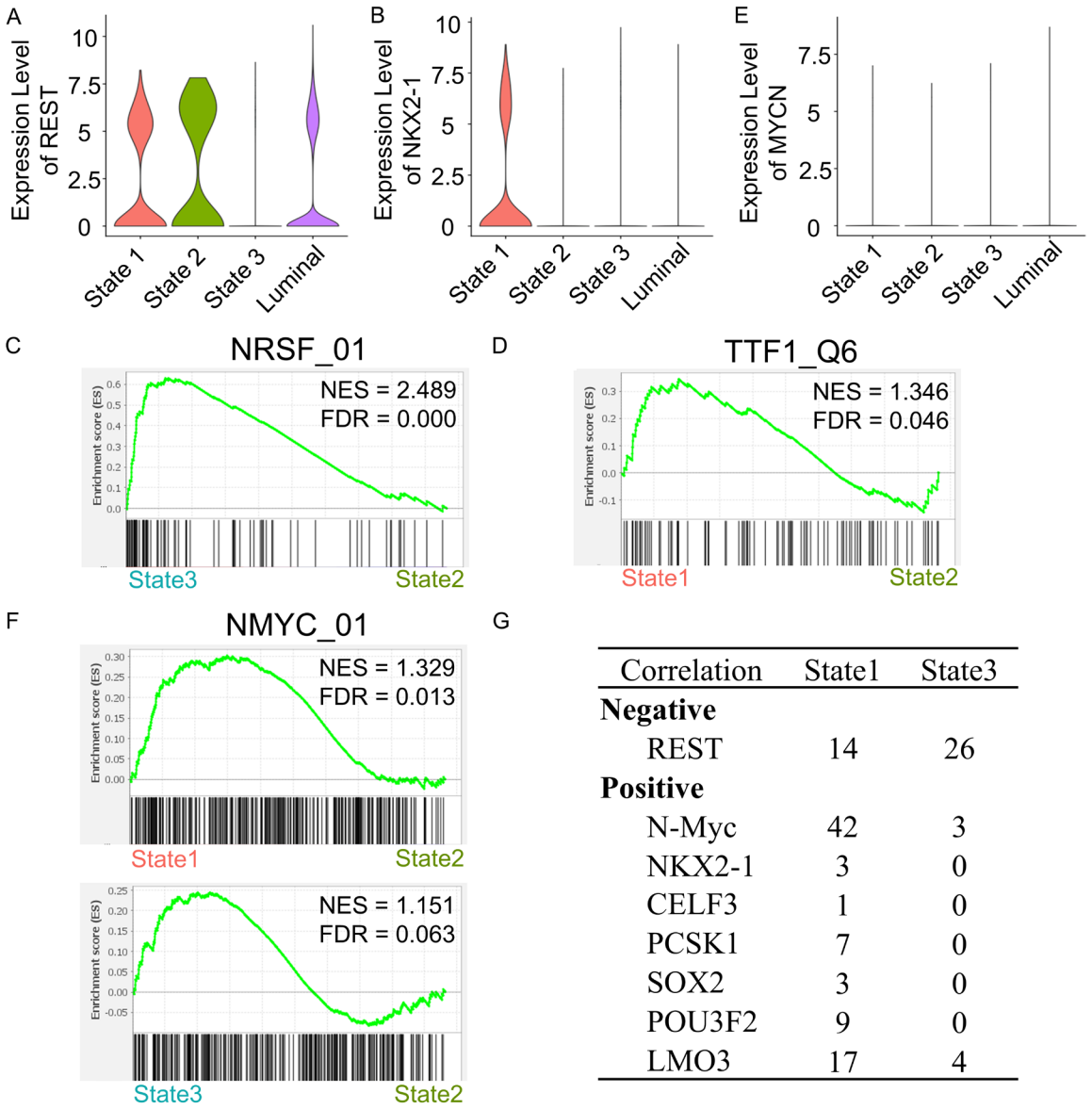

G

Correlation	State1	State3
Negative		
REST	14	26
Positive		
N-Myc	42	3
NKX2-1	3	0
CELF3	1	0
PCSK1	7	0
SOX2	3	0
POU3F2	9	0
LMO3	17	4

Figure 5. Gene set enrichment analysis (GSEA) identifies REST and N-Myc as potential master transcriptional regulators in different states of NEPC. (A and B) The violin plots display the expression of REST (A) and NKX2-1 (B) in states 1, 2, 3 and the luminal group. (C and D) Enrichment plots of REST (NRSF_01) (C) and NKX2-1 (TTF_Q6) (D) gene sets between the indicated states. (E) The violin plot displays the expression of N-Myc in states 1, 2, 3 and luminal group. (F) Enrichment plots of N-Myc (NMYC_01) gene set between the indicated states. (G) Table of the number of genes in states 1 and 3 that showed a statistically significant negative correlation with REST and positive correlation with N-Myc, NKX2-1, CELF3, PCSK1, SOX2, POU3F2, and LMO3.

found in the TCGA database, and 42 of them were positively correlated with N-Myc, while only a few of them were positively correlated with the NEURO II transcription factors (**Figure 5G**). On the contrary, among the 392 of 406 biomarkers in state 3 (Table S2) identified in TCGA, only 3 and 4 of them were positively correlated with N-Myc and LMO3, respectively, while no gene was found to correlate with other NEURO II transcription factors (**Figure 5G**). These analyses together supported the notion that N-Myc is the key epigenetic regulator that mediated the lineage plasticity of NEPC state 1. Given that NKX2-1 is a downstream target of N-Myc and N-Myc (**Figure 5F**, upper panel) showed a higher significance enrichment than NKX2-1 (**Figure 5D**) in GSEA, a possible explanation is that induction of N-Myc may initiate

the plasticity of PCA cells through distinct epigenetic mechanisms, allowing NEPC cells switched toward state 1. This interpretation can also support by the bulk RNA-seq data of CRPC from Labrecque *et al.* published in 2019, showing that NE-associated transcription factors regulate a distinct neuroendocrine phenotype (NEURO II) [23]. Therefore, we concluded that during NED, luminal cells start with lose of AR signaling and subsequently undergo either REST-mediated or N-Myc-mediated epigenetic reprogramming in CRPC.

N-Myc-driven NEPC is critical for PCA diagnosis and prognosis

To elucidate the clinical relevance of NEPC states mediated by N-Myc and REST, the correlations of NEPC states 1 and 3 were analyzed with the expression patterns of their biomarkers in PCA patients from TCGA. Strikingly, most of the biomarkers in state 1 were highly expressed in PCA tissues, especially in patients with a Gleason score greater than 8 (**Figure 6A**, upper panel). On the other hand, the expression levels of most state 3 biomarkers (Table S2) in normal prostate were similar to those in PCA tissues (**Figure 6A**, lower panel). This suggests a higher potential of N-Myc-driven NEPC in distinguishing normal prostate from high-grade PCA. To validate this, we also performed ROC analysis of the top 10 most significant biomarker genes in NEPC state 1 and state 3. In line with our hypothesis, ROC analysis showed that all of the top 10 biomarkers in N-Myc-driven state (state 1) exhibited high specificity and sensitivity in distinguishing PCA from normal tissue, while only two of the top 10 biomarkers in REST-driven state (state 3) showed distinguishing ability (**Figure 6B** and **6C**).

To determine the potential roles of N-Myc-driven NEPC in the progression of PCA, functional enrichment analysis was performed using IPA. Biomarker genes in NEPC state 1 were mainly enriched for cell proliferation and survival-related processes involved in cancer progression, such as positive regulation (z-score > 2.5; red) of cell proliferation and survival and negative regulation (z-score < -2.5; blue) of apoptosis and senescence, indicating the malignancy of NEPC state 1 (**Figure 7A**). Furthermore, since numerous patients with CRPC relapse into NEPC, we further evaluated whether NEPC state 1 contributes to PCA recurrence. Consistent with our hypothesis, Kaplan-Meier analysis using GEPIA revealed that all of the top 10 biomarkers in state 1 showed significant abilities to predict disease-free survival in terms of recurrence (**Figure 7B**), while only one of the top 10 biomarkers in REST-driven state (C20orf204) showed distinguishing ability (**Figure 7C**). A more important finding was the negative enrichment in the sensitivity of cells in response to therapeutics (**Figure 7A**). Since therapeutic resistance accounts for most CRPC-related deaths, this data suggests that state 1 may be related to drug resistance of CRPC. In summary, malignant cells in NEPC state 1 are critical for the diagnosis and prognosis of PCA.

Discussion

Drug resistance in cancer is often linked to mutations in drug-target, but growing transcriptomic analyses indicate that CRPC, a highly heterogeneous tumor sharing features of normal development, may escape next-generation AR pathway inhibitors designed to circumvent AR-based resistance through lineage transition from prostate adenocarcinoma to NEPC [3, 5, 38]. Therefore, it is believed that lineage plasticity may play a causal role in the development of resistance to ARI and the incidence of NEPC has increased coinciding with the wildly use of second-line ARIs over the past decade [35]. Consistent with this, whole-exome sequencing of mCRPC biopsies revealed that epigenetic modifiers, but not genetic alteration, play a key role in the induction and/or maintenance of the treatment-resistant state of NEPC [39]. More interestingly, studies of mCRPC have been extensively performed with bulk RNA-seq and highlight the central role of AR and REST in treatment-resistant CRPC [23]. Here, we performed an in-depth scRNA-seq in a lymph node mCRPC specimen from a recurrent patient who had previous bone metastases (in 2016 and 2019) and received prior ADT therapy. Of note, we identified a distinct NEPC population, with a significantly higher expression of REST-repressed genes (**Figure 2F**). Thus, for the first time, our finding has proven REST that has been long proposed to explain NED in PCA [21-23] as a potential transcription repressor for NEPC at single cell resolution in a human specimen.

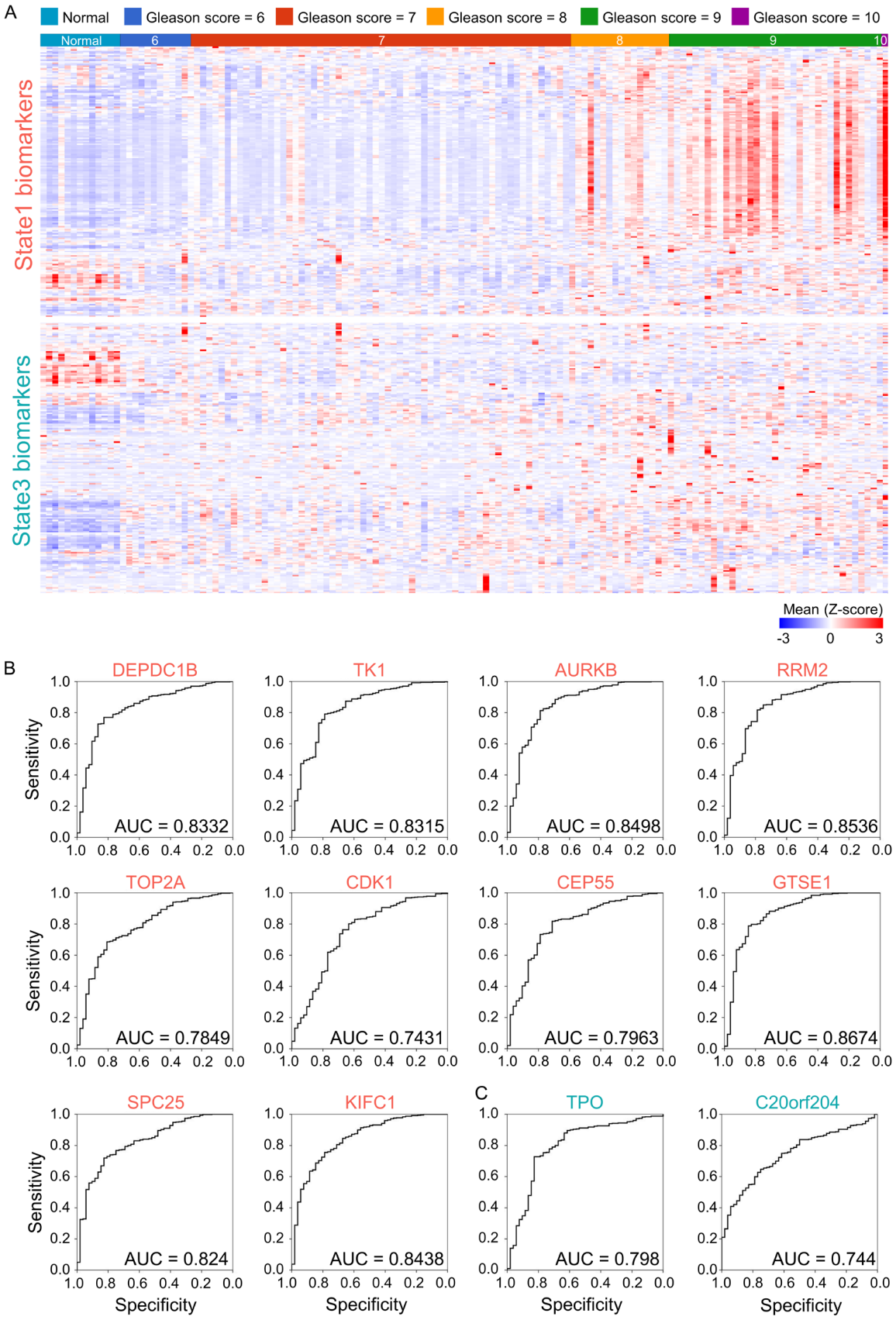

Figure 6. Clinical relevance of NEPC states 1 and 3 for PCA diagnosis. A. Heatmap demonstrating the correlation of PCA status with state 1 (top) and state 3 (bottom) biomarker gene expression using TCGA dataset. B. ROC curves for

the top 10 biomarker genes in state 1 in distinguishing normal prostate and PCA using TCGA dataset. C. ROC curves for two of the top 10 biomarker genes in state 3 that can distinguish normal prostate from cancerous prostate using TCGA dataset.

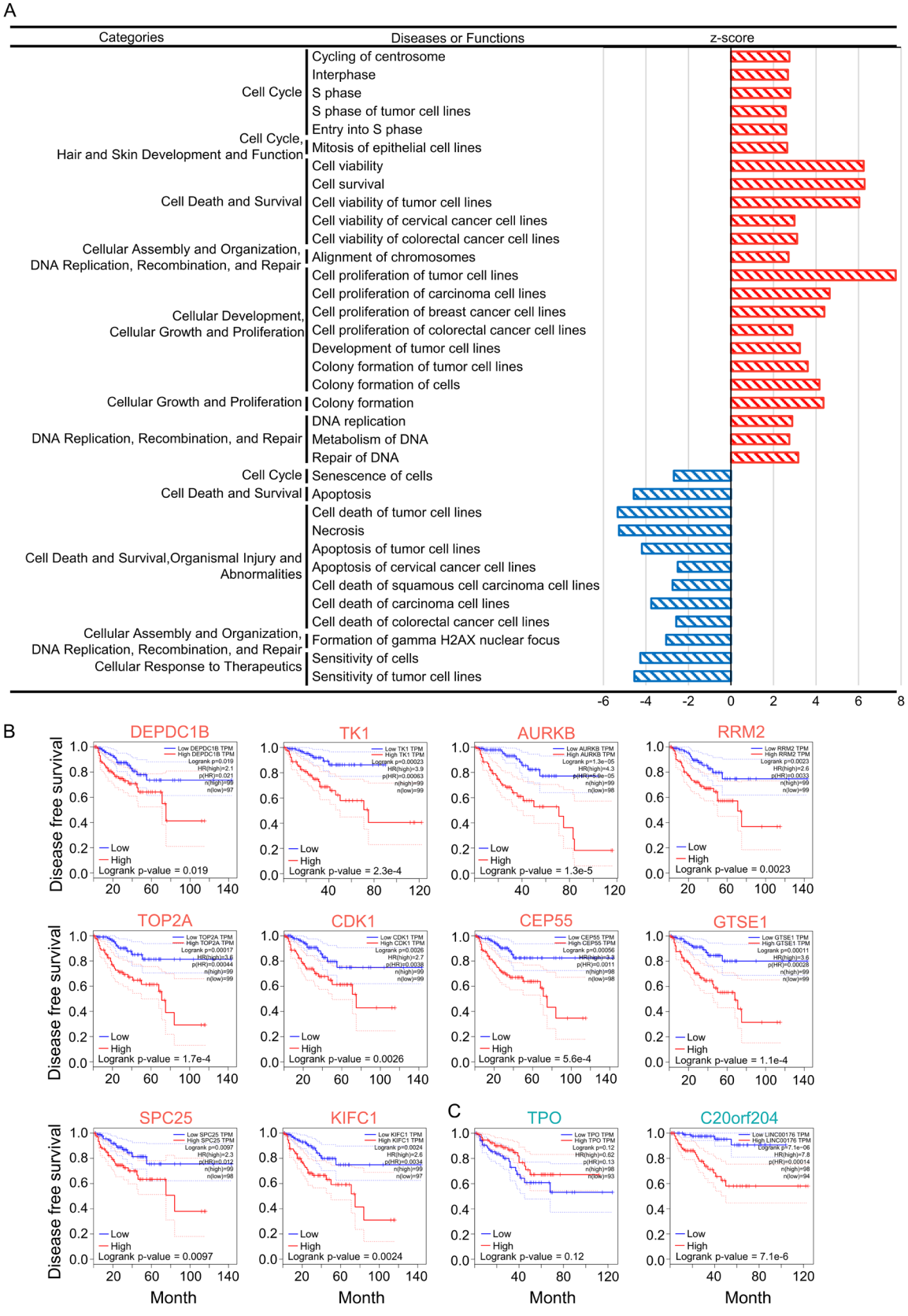

Figure 7. Identification of cell properties in NEPC states 1. A. IPA was used to reveal functional categories significantly enriched in the biomarker genes of NEPC state 1. B. Kaplan-Meier analysis was performed using Gene Expression Profiling Interactive Analysis (GEPIA) to predict the recurrence-free survival in PCA patients according to the expression levels of the top 10 biomarker genes of state 1. C. Kaplan-Meier analysis of the two biomarker genes in state 3 (**Figure 6C**). The Mantel-Cox test was used to calculate the logarithmic rank *p*-value (*p*-value in each plot).

scRNA-seq analysis is a powerful tool for characterizing the transcriptional profiles of tumor specimens at the single-cell level and has been instructive in revealing heterogeneities within and between PCA patients [28-31, 40]. However, the heterogeneity of NEPC has never been in-depth studied in single-cell level. This may due to the fact that NEPC population is typically present in the minority and does not universally exist in all CRPC specimens [28, 30, 31]. Therefore, it is difficult to precisely decipher their transdifferentiation mechanism, particularly in combined sample analysis, due to the presence of the large number of CRPC-adeno cells. More importantly, although epigenetic factors, such as N-Myc, and REST, have been implicated in neuroendocrine transdifferentiation of prostate adenocarcinoma cells, their role in mediating the heterogeneity of NEPC has never been studied at the single-cell level. In this study, by using the strategy of combining neuroendocrine clusters from individual samples, we have successfully elucidated different states of NEPC cells, with a state regulated by N-Myc and a state regulated by REST.

Recently, scRNA-seq has also been applied to profile the heterogeneity of CRPC. Dong *et al.* performed a scRNA-seq on six CRPC specimens and identified luminal-neuroendocrine transdifferentiation in four of them [30]. In combination with CRPC samples from Dong's group, Wang *et al*. found two NEPC gene expression signatures, including NE1 that expressed a high level of ASCL1 and NE2 that expressed a high level of CHGA, CHGB, and ENO2, representing the early and late state of the NED process, respectively. Although distinct transcriptomic profiles have been revealed in NEPC cells, studies using scRNA-seq to elucidate epigenetic drivers have not yet been reported.

In this study, we conducted a trajectory analysis of NEPC cells collected from one CRPC, three CRPC with metastasis and one lymph node mCRPC specimens (**Figure 3**) and identified three cells states, with one initial (state 2) and two distinct neuroendocrine states (state 1 and state 3) (**Figure 4**). We found that REST expression was lost in one neuroendocrine state (state 3) (**Figure 5A**). This result further confirmed REST as a key transcription repressor for NEPC. However, most of the transcription factors known to be associated with NED were not detected in the scRNA-seq. A possible reason for this is that most transcription factors are expressed at low levels inside cells and are difficult to detect by scRNA-seq. However, although the mRNA levels of transcription factors may be low, the expression of their target genes can be high after the induction. Therefore, we employed a functional enrichment analysis approach using a transcription factor-targeted gene set. Given that Labrecque *et al.* performed bulk RNA-seq in 98 treatment-refractory mCRPC and divided neuroendocrine-associated genes into REST-repressed genes (NEURO I) and transcription factors (NEURO II), we performed GSEA in REST and three NEURO II-associated transcription factors, NKX2-1, SOX2, and POU3F2, with an available target gene set. Consistently, a significant enrichment of REST-targeted genes with state 3 was identified (**Figure 5C**). Notably, a slight but significant association was found in NKX2-1 (FDR=0.046), but not in SOX2 (FDR=0.187) nor in POU3F2 (FDR=0.052). This result suggested that the NED of NEPC state 3 could be determined by a higher stratum of transcription factors other than the transcription factors in NEURO II [23].

Since an integrated transcriptomics analysis of PCA and genetically modified mouse models revealed the central role of N-Myc in NEPC in 2016 [18, 19], N-Myc is nowadays recognized as a key epigenetic activator driving the lineage plasticity of NEPC [12, 37]. Given that NKX2-1, the only NEURO II transcription factor associated with NEPC state 1 (**Figure 5D**), is a downstream target of N-Myc [12], we studied the enrichment of N-Myc target genes in state 1 using GSEA. N-Myc target genes in state 3 were also analyzed and used as a control. Consistent with our hypothesis, a significant enrichment of N-Myc target genes was found in state 1 (FDR=0.013), but not in state 3 (FDR=0.063) (**Figure 5F**). To elucidate the importance of N-Myc in gene expression in state 1, we further

calculated the correlation between N-Myc and biomarker genes in state 1 using the TCGA dataset (Table S1). The other transcription factors in NEURO II were also analyzed in parallel to distinguish the effect caused by N-Myc or other transcription factors. Among the 392 biomarkers found in the TCGA database, 42 of them (10.7%) were positively correlated with N-Myc, while only 3 (0.8%), 1 (0.3%), 7 (1.8%), 3 (0.8%), 9 (2.3%), and 17 (4.3%) biomarkers in state 3 were correlated with NKX2-1, CELF3, PCSK1, SOX2, POU3F2, and LMO3, respectively (**Figure 5G**). Interesting, only 3 (0.8%) and 4 (1%) of biomarkers in state 3 were positively correlated with N-Myc and LMO3, respectively, and no biomarkers were found to correlate with the other transcription factors of NEURO II (**Figure 5G**). Collectively, these data not only supported the existence of state-specific transcriptional factors in NEPC states 1 and 3, but more importantly showed us that N-Myc as a key transcription regulator of a state of NEPC cells. It should be noted that our results do not exclude the possibility that state 1 of NEPC may also be regulated by other transcription factors. To our knowledge, this is the first report of NEPC heterogeneity and transcription factor activities examined by scRNA-seq of CRPC tissue.

Another fundamental problem of NEPC is the inability to diagnose the disease early and accurately. To achieve an early diagnosis, it is crucial to identify feasible biomarkers that can detect the emergence of NEPC. In this study, CgA, a classical neuroendocrine biomarker used in clinical practice [24], was detected in the REST-regulated state (state 3). Unexpectedly, the biomarkers detected in this state have poor predictive ability in PCA patients. Interestingly, most biomarkers in the Myc-regulated state (state 1) were highly expressed in PCA tissues, especially in PCA with a Gleason score above 8 (**Figure 6A**, upper panel). Furthermore, all of the top 10 biomarkers in the N-Myc-regulated state exhibited high specificity and sensitivity in the diagnosis of PCA (**Figure 6B**) and showed significant abilities to predict PCA recurrence (**Figure 7B**). Since PCA specimens in TCGA are mostly prostate adenocarcinoma (TCGA-PRAD), the biomarker genes that we identified in N-Myc-regulated state may represent early diagnostic biomarkers for NEPC. Taken together, the biomarkers identified in this study may help monitor the early "critical period" of the onset of NEPC, during which therapies could prevent, delay, or even reverse plasticity.

Taken together, we elucidated N-Myc and REST as two master regulators in mediating lineage plasticity and classifying neuroendocrine phenotypes. Given that the unique biomarkers identified in the neuroendocrine subtype could potentially guide future diagnosis and treatment of the highly lethal AR-independent CRPC, the biomarkers identified in this study may help monitor the early "critical period" of the onset of NEPC, during which therapies could prevent, delay, or even reverse plasticity.

Acknowledgements

The authors acknowledge the "technical services" provided by the Genomics Center for Clinical and Biotechnological Applications of the Cancer Progression Research Center (National Yang Ming Chiao Tung University). The National Core Facility for Biopharmaceuticals (NCFB), Ministry of Science and Technology. The work was supported by grants to T.P.L. (MOST 106-2314-B-075-053-MY3 and 109-2314-B-075-072-MY3; NSTC 112-2314-B-A49-055-MY3; NHRI NHRI-109BCCO-MF-202014-03; Taipei Veterans General Hospital, V109C-111, V110C-104, V111C-081, V112C-077; and Yen Ching Ling Medical Foundation, CI-106-17 and CI-110-21) and grants to P.C.C. (MOST 108-2320-B-010-029-MY3 and 111-2320-B-A49-030-MY3; NHRI NHRI-EX111~113-111-25BI). This work was supported by grants from the Ministry of Education, Higher Education SPROUT Project for Cancer Progression Research Center (111W31101) and Cancer and Immunology Research Center (112W31101).

Disclosure of conflict of interest

None.

Address correspondence to: Tzu-Ping Lin, Department of Urology, Taipei Veterans General Hospital, Taipei 11217, Taiwan. Tel: +886-2-2875-7519; E-mail: tplin@vghtpe.gov.tw

References

[1] Bray F, Ferlay J, Soerjomataram I, Siegel RL, Torre LA and Jemal A. Global cancer statistics 2018: GLOBOCAN estimates of incidence and mortality worldwide for 36 cancers in 185

countries. CA Cancer J Clin 2018; 68: 394-424.
[2] Huggins C. Effect of orchiectomy and irradiation on cancer of the prostate. Ann Surg 1942; 115: 1192-1200.
[3] Watson PA, Arora VK and Sawyers CL. Emerging mechanisms of resistance to androgen receptor inhibitors in prostate cancer. Nat Rev Cancer 2015; 15: 701-711.
[4] Loriot Y, Bianchini D, Ileana E, Sandhu S, Patrikidou A, Pezaro C, Albiges L, Attard G, Fizazi K, De Bono JS and Massard C. Antitumour activity of abiraterone acetate against metastatic castration-resistant prostate cancer progressing after docetaxel and enzalutamide (MDV3100). Ann Oncol 2013; 24: 1807-1812.
[5] Davies AH, Beltran H and Zoubeidi A. Cellular plasticity and the neuroendocrine phenotype in prostate cancer. Nat Rev Urol 2018; 15: 271-286.
[6] Puca L, Vlachostergios PJ and Beltran H. Neuroendocrine differentiation in prostate cancer: emerging biology, models, and therapies. Cold Spring Harb Perspect Med 2019; 9: a030593.
[7] Aggarwal R, Huang J, Alumkal JJ, Zhang L, Feng FY, Thomas GV, Weinstein AS, Friedl V, Zhang C, Witte ON, Lloyd P, Gleave M, Evans CP, Youngren J, Beer TM, Rettig M, Wong CK, True L, Foye A, Playdle D, Ryan CJ, Lara P, Chi KN, Uzunangelov V, Sokolov A, Newton Y, Beltran H, Demichelis F, Rubin MA, Stuart JM and Small EJ. Clinical and genomic characterization of treatment-emergent small-cell neuroendocrine prostate cancer: a multi-institutional prospective study. J Clin Oncol 2018; 36: 2492-2503.
[8] Rickman DS, Beltran H, Demichelis F and Rubin MA. Biology and evolution of poorly differentiated neuroendocrine tumors. Nat Med 2017; 23: 1-10.
[9] Nijhout HF. Development and evolution of adaptive polyphenisms. Evol Dev 2003; 5: 9-18.
[10] Boumahdi S and de Sauvage FJ. The great escape: tumour cell plasticity in resistance to targeted therapy. Nat Rev Drug Discov 2020; 19: 39-56.
[11] Beltran H, Hruszkewycz A, Scher HI, Hildesheim J, Isaacs J, Yu EY, Kelly K, Lin D, Dicker A, Arnold J, Hecht T, Wicha M, Sears R, Rowley D, White R, Gulley JL, Lee J, Diaz Meco M, Small EJ, Shen M, Knudsen K, Goodrich DW, Lotan T, Zoubeidi A, Sawyers CL, Rudin CM, Loda M, Thompson T, Rubin MA, Tawab-Amiri A, Dahut W and Nelson PS. The role of lineage plasticity in prostate cancer therapy resistance. Clin Cancer Res 2019; 25: 6916-6924.
[12] Berger A, Brady NJ, Bareja R, Robinson B, Conteduca V, Augello MA, Puca L, Ahmed A, Dardenne E, Lu X, Hwang I, Bagadion AM, Sboner A, Elemento O, Paik J, Yu J, Barbieri CE, Dephoure N, Beltran H and Rickman DS. N-Myc-mediated epigenetic reprogramming drives lineage plasticity in advanced prostate cancer. J Clin Invest 2019; 129: 3924-3940.
[13] Cyrta J, Augspach A, De Filippo MR, Prandi D, Thienger P, Benelli M, Cooley V, Bareja R, Wilkes D, Chae SS, Cavaliere P, Dephoure N, Uldry AC, Lagache SB, Roma L, Cohen S, Jaquet M, Brandt LP, Alshalalfa M, Puca L, Sboner A, Feng F, Wang S, Beltran H, Lotan T, Spahn M, Kruithof-de Julio M, Chen Y, Ballman KV, Demichelis F, Piscuoglio S and Rubin MA. Role of specialized composition of SWI/SNF complexes in prostate cancer lineage plasticity. Nat Commun 2020; 11: 5549.
[14] Beltran H, Tomlins S, Aparicio A, Arora V, Rickman D, Ayala G, Huang J, True L, Gleave ME, Soule H, Logothetis C and Rubin MA. Aggressive variants of castration-resistant prostate cancer. Clin Cancer Res 2014; 20: 2846-2850.
[15] Ku SY, Rosario S, Wang Y, Mu P, Seshadri M, Goodrich ZW, Goodrich MM, Labbe DP, Gomez EC, Wang J, Long HW, Xu B, Brown M, Loda M, Sawyers CL, Ellis L and Goodrich DW. Rb1 and Trp53 cooperate to suppress prostate cancer lineage plasticity, metastasis, and antiandrogen resistance. Science 2017; 355: 78-83.
[16] Martin P, Liu YN, Pierce R, Abou-Kheir W, Casey O, Seng V, Camacho D, Simpson RM and Kelly K. Prostate epithelial Pten/TP53 loss leads to transformation of multipotential progenitors and epithelial to mesenchymal transition. Am J Pathol 2011; 179: 422-435.
[17] Beltran H, Rickman DS, Park K, Chae SS, Sboner A, MacDonald TY, Wang Y, Sheikh KL, Terry S, Tagawa ST, Dhir R, Nelson JB, de la Taille A, Allory Y, Gerstein MB, Perner S, Pienta KJ, Chinnaiyan AM, Wang Y, Collins CC, Gleave ME, Demichelis F, Nanus DM and Rubin MA. Molecular characterization of neuroendocrine prostate cancer and identification of new drug targets. Cancer Discov 2011; 1: 487-495.
[18] Dardenne E, Beltran H, Benelli M, Gayvert K, Berger A, Puca L, Cyrta J, Sboner A, Noorzad Z, MacDonald T, Cheung C, Yuen KS, Gao D, Chen Y, Eilers M, Mosquera JM, Robinson BD, Elemento O, Rubin MA, Demichelis F and Rickman DS. N-Myc induces an EZH2-mediated transcriptional program driving neuroendocrine prostate cancer. Cancer Cell 2016; 30: 563-577.
[19] Lee JK, Phillips JW, Smith BA, Park JW, Stoyanova T, McCaffrey EF, Baertsch R, Sokolov A, Meyerowitz JG, Mathis C, Cheng D, Stuart JM, Shokat KM, Gustafson WC, Huang J and Witte ON. N-Myc drives neuroendocrine prostate

cancer initiated from human prostate epithelial cells. Cancer Cell 2016; 29: 536-547.
[20] Sidaway P. Prostate cancer: N-Myc expression drives neuroendocrine disease. Nat Rev Urol 2016; 13: 695.
[21] Chang PC, Wang TY, Chang YT, Chu CY, Lee CL, Hsu HW, Zhou TA, Wu Z, Kim RH, Desai SJ, Liu S and Kung HJ. Autophagy pathway is required for IL-6 induced neuroendocrine differentiation and chemoresistance of prostate cancer LNCaP cells. PLoS One 2014; 9: e88556.
[22] Svensson C, Ceder J, Iglesias-Gato D, Chuan YC, Pang ST, Bjartell A, Martinez RM, Bott L, Helczynski L, Ulmert D, Wang Y, Niu Y, Collins C and Flores-Morales A. REST mediates androgen receptor actions on gene repression and predicts early recurrence of prostate cancer. Nucleic Acids Res 2014; 42: 999-1015.
[23] Labrecque MP, Coleman IM, Brown LG, True LD, Kollath L, Lakely B, Nguyen HM, Yang YC, da Costa RMG, Kaipainen A, Coleman R, Higano CS, Yu EY, Cheng HH, Mostaghel EA, Montgomery B, Schweizer MT, Hsieh AC, Lin DW, Corey E, Nelson PS and Morrissey C. Molecular profiling stratifies diverse phenotypes of treatment-refractory metastatic castration-resistant prostate cancer. J Clin Invest 2019; 129: 4492-4505.
[24] Epstein JI, Amin MB, Beltran H, Lotan TL, Mosquera JM, Reuter VE, Robinson BD, Troncoso P and Rubin MA. Proposed morphologic classification of prostate cancer with neuroendocrine differentiation. Am J Surg Pathol 2014; 38: 756-767.
[25] Priemer DS, Montironi R, Wang L, Williamson SR, Lopez-Beltran A and Cheng L. Neuroendocrine tumors of the prostate: emerging insights from molecular data and updates to the 2016 World Health Organization Classification. Endocr Pathol 2016; 27: 123-135.
[26] Lawson DA, Bhakta NR, Kessenbrock K, Prummel KD, Yu Y, Takai K, Zhou A, Eyob H, Balakrishnan S, Wang CY, Yaswen P, Goga A and Werb Z. Single-cell analysis reveals a stem-cell program in human metastatic breast cancer cells. Nature 2015; 526: 131-135.
[27] Tirosh I, Izar B, Prakadan SM, Wadsworth MH 2nd, Treacy D, Trombetta JJ, Rotem A, Rodman C, Lian C, Murphy G, Fallahi-Sichani M, Dutton-Regester K, Lin JR, Cohen O, Shah P, Lu D, Genshaft AS, Hughes TK, Ziegler CG, Kazer SW, Gaillard A, Kolb KE, Villani AC, Johannessen CM, Andreev AY, Van Allen EM, Bertagnolli M, Sorger PK, Sullivan RJ, Flaherty KT, Frederick DT, Jane-Valbuena J, Yoon CH, Rozenblatt-Rosen O, Shalek AK, Regev A and Garraway LA. Dissecting the multicellular ecosystem of metastatic melanoma by single-cell RNA-seq. Science 2016; 352: 189-196.
[28] Ma X, Guo J, Liu K, Chen L, Liu D, Dong S, Xia J, Long Q, Yue Y, Zhao P, Hu F, Xiao Z, Pan X, Xiao K, Cheng Z, Ke Z, Chen ZS and Zou C. Identification of a distinct luminal subgroup diagnosing and stratifying early stage prostate cancer by tissue-based single-cell RNA sequencing. Mol Cancer 2020; 19: 147.
[29] Song H, Weinstein HNW, Allegakoen P, Wadsworth MH 2nd, Xie J, Yang H, Castro EA, Lu KL, Stohr BA, Feng FY, Carroll PR, Wang B, Cooperberg MR, Shalek AK and Huang FW. Single-cell analysis of human primary prostate cancer reveals the heterogeneity of tumor-associated epithelial cell states. Nat Commun 2022; 13: 141.
[30] Dong B, Miao J, Wang Y, Luo W, Ji Z, Lai H, Zhang M, Cheng X, Wang J, Fang Y, Zhu HH, Chua CW, Fan L, Zhu Y, Pan J, Wang J, Xue W and Gao WQ. Single-cell analysis supports a luminal-neuroendocrine transdifferentiation in human prostate cancer. Commun Biol 2020; 3: 778.
[31] Wang Z, Wang T, Hong D, Dong B, Wang Y, Huang H, Zhang W, Lian B, Ji B, Shi H, Qu M, Gao X, Li D, Collins C, Wei G, Xu C, Lee HJ, Huang J and Li J. Single-cell transcriptional regulation and genetic evolution of neuroendocrine prostate cancer. iScience 2022; 25: 104576.
[32] Chen S, Zhu G, Yang Y, Wang F, Xiao YT, Zhang N, Bian X, Zhu Y, Yu Y, Liu F, Dong K, Mariscal J, Liu Y, Soares F, Loo Yau H, Zhang B, Chen W, Wang C, Chen D, Guo Q, Yi Z, Liu M, Fraser M, De Carvalho DD, Boutros PC, Di Vizio D, Jiang Z, van der Kwast T, Berlin A, Wu S, Wang J, He HH and Ren S. Single-cell analysis reveals transcriptomic remodellings in distinct cell types that contribute to human prostate cancer progression. Nat Cell Biol 2021; 23: 87-98.
[33] He MX, Cuoco MS, Crowdis J, Bosma-Moody A, Zhang Z, Bi K, Kanodia A, Su MJ, Ku SY, Garcia MM, Sweet AR, Rodman C, DelloStritto L, Silver R, Steinharter J, Shah P, Izar B, Walk NC, Burke KP, Bakouny Z, Tewari AK, Liu D, Camp SY, Vokes NI, Salari K, Park J, Vigneau S, Fong L, Russo JW, Yuan X, Balk SP, Beltran H, Rozenblatt-Rosen O, Regev A, Rotem A, Taplin ME and Van Allen EM. Transcriptional mediators of treatment resistance in lethal prostate cancer. Nat Med 2021; 27: 426-433.
[34] Zhang X, Lan Y, Xu J, Quan F, Zhao E, Deng C, Luo T, Xu L, Liao G, Yan M, Ping Y, Li F, Shi A, Bai J, Zhao T, Li X and Xiao Y. CellMarker: a manually curated resource of cell markers in human and mouse. Nucleic Acids Res 2019; 47: D721-D728.
[35] Bluemn EG, Coleman IM, Lucas JM, Coleman RT, Hernandez-Lopez S, Tharakan R, Bianchi-Frias D, Dumpit RF, Kaipainen A, Corella AN,

Yang YC, Nyquist MD, Mostaghel E, Hsieh AC, Zhang X, Corey E, Brown LG, Nguyen HM, Pienta K, Ittmann M, Schweizer M, True LD, Wise D, Rennie PS, Vessella RL, Morrissey C and Nelson PS. Androgen receptor pathway-independent prostate cancer is sustained through FGF signaling. Cancer Cell 2017; 32: 474-489. e6.

[36] Conteduca V, Aieta M, Amadori D and De Giorgi U. Neuroendocrine differentiation in prostate cancer: current and emerging therapy strategies. Crit Rev Oncol Hematol 2014; 92: 11-24.

[37] Yin Y, Xu L, Chang Y, Zeng T, Chen X, Wang A, Groth J, Foo WC, Liang C, Hu H and Huang J. N-Myc promotes therapeutic resistance development of neuroendocrine prostate cancer by differentially regulating miR-421/ATM pathway. Mol Cancer 2019; 18: 11.

[38] Quintanal-Villalonga A, Chan JM, Yu HA, Pe'er D, Sawyers CL, Sen T and Rudin CM. Lineage plasticity in cancer: a shared pathway of therapeutic resistance. Nat Rev Clin Oncol 2020; 17: 360-371.

[39] Beltran H, Prandi D, Mosquera JM, Benelli M, Puca L, Cyrta J, Marotz C, Giannopoulou E, Chakravarthi BV, Varambally S, Tomlins SA, Nanus DM, Tagawa ST, Van Allen EM, Elemento O, Sboner A, Garraway LA, Rubin MA and Demichelis F. Divergent clonal evolution of castration-resistant neuroendocrine prostate cancer. Nat Med 2016; 22: 298-305.

[40] Ge G, Han Y, Zhang J, Li X, Liu X, Gong Y, Lei Z, Wang J, Zhu W, Xu Y, Peng Y, Deng J, Zhang B, Li X, Zhou L, He H and Ci W. Single-cell RNA-seq reveals a developmental hierarchy superimposed over subclonal evolution in the cellular ecosystem of prostate cancer. Adv Sci (Weinh) 2022; 9: e2105530.

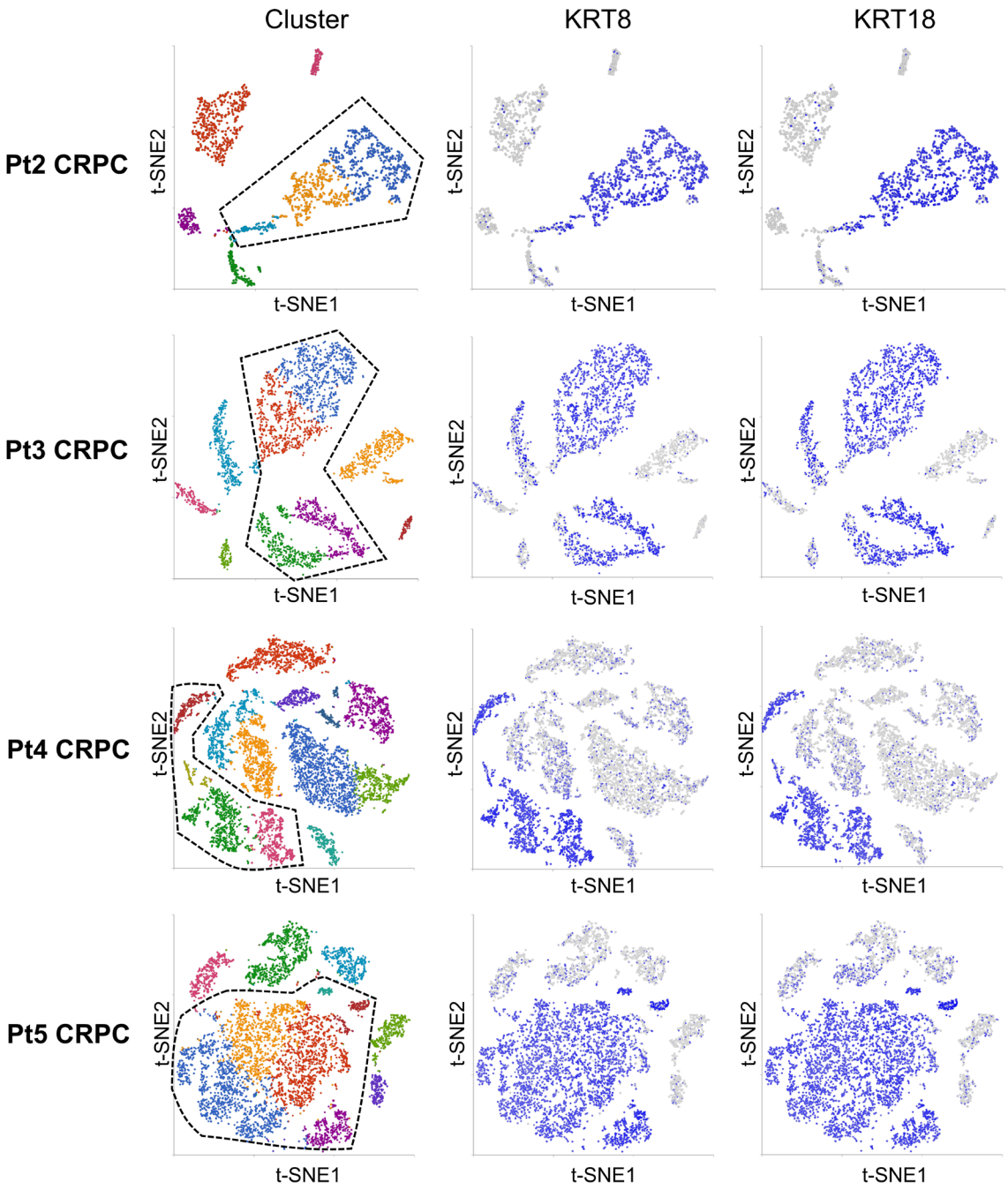

Figure S1. t-SNE plot of cells from four patients with CRPC (left column) with cells colored according to the luminal marker genes KRT8 (middle column) and KRT18 (right column).